The Astrophysical Journal, 577:951–960, 2002 October 1

NEW CHALLENGES FOR WIND SHOCK MODELS: THE *CHANDRA* SPECTRUM OF THE HOT STAR δ ORIONIS

N. A. Miller,[1] J. P. Cassinelli,[1] W. L. Waldron,[2] J. J. MacFarlane,[3] and D. H. Cohen[3,4]

Received 2001 June 19; accepted 2002 June 3

ABSTRACT

The *Chandra* spectrum of δ Ori A shows emission lines from hydrogen- and helium-like states of Si, Mg, Ne, and O, along with N VII Lyα and lines from ions in the range Fe XVII–Fe XXI. In contrast to the broad lines seen in ζ Pup and ζ Ori (850 ± 40 and 1000 ± 240 km s^{-1} half-width at half-maximum [HWHM], respectively), these lines are broadened to only 430 ± 60 km s^{-1} HWHM. This is much lower than the measured wind terminal velocity of 2000 km s^{-1}. The forbidden, intercombination, and resonance (*fir*) lines from He-like ions indicate that the majority of the X-ray line emission does not originate at the base of the wind, in agreement with the standard wind shock models for these objects. However, in that model the X-ray emission is distributed throughout an expanding, X-ray–absorbing wind, and it is therefore surprising that the emission lines appear relatively narrow, unshifted, and symmetric. We compare the observed line profiles to recent detailed models for X-ray line profile generation in hot stars, but none of them offers a fully satisfactory explanation for the observed line profiles.

Subject headings: line: profiles — stars: early-type — stars: individual (δ Orionis) — stars: mass loss — stars: winds, outflows — X-rays: stars

1. INTRODUCTION

Nearly all O and many early B stars are soft X-ray sources (Berghöfer et al. 1997). The origin of these X-rays is still not well understood, even after 20 yr of observations. The principal model developed to explain these X-ray observations envisions small instabilities in the powerful outflowing winds of these hot stars quickly growing into strong reverse shocks. The result is hot, widely distributed X-ray–emitting gas. In this model, the wind consists of two components: While most of the wind is cool (at roughly photospheric temperatures), a small portion of the wind is heated to X-ray–emitting temperatures by the wind shocks. This basic model, originated by Lucy & White (1980), has been developed through a series of papers by various authors, including Lucy (1982), Owocki, Castor, & Rybicki (1988), Cooper & Owocki (1994), Owocki & Puls (1996, 1999), Runacres & Owocki (2002), and a series of papers by Feldmeier (Feldmeier 1995; Feldmeier et al. 1997a; Feldmeier, Puls, & Pauldrach 1997b; Feldmeier 2001).[5] In Feldmeier's models, the shocks themselves do not produce strong enough X-ray emission to match observations. Rather, it is the collisions between shocks that result in clumps dense enough to explain the X-ray emission. More specifically, at any given time in his one-dimensional simulations, most of the X-rays are emitted from a single shock (Feldmeier 1995). This region of emission is a location in which a small, fast-moving shock cloudlet has caught up to larger, more slowly moving shock (Feldmeier 2001).

[1] Astronomy Department, University of Wisconsin, 475 North Charter Street, Madison, WI 53706; nmiller@astro.wisc.edu, cassinelli@astro.wisc.edu.

[2] L-3 Communications Analytics Corporation, 1801 McCormick Drive, Suite 170, Largo, MD 20774; wayne.waldron@L-3com.com.

[3] Prism Computational Sciences, 16 North Carroll Street, Madison, WI 53703; jjm@prism-cs.com.

[4] Department of Physics and Astronomy, Swarthmore College, Swarthmore, PA 19081; dcohen1@swarthmore.edu.

[5] Thesis information is available from http://auriga.astro.physik.uni-potsdam.de/~afeld/habil.html.

The Orion belt star δ Ori has long been an important target in the quest to determine the cause of early-type stellar X-ray emission. It is now one of the few early-type stars to have been observed at the high resolution possible with X-ray–grating spectrographs. An early spectrum of this star was obtained by Cassinelli & Swank (1983) in their *Einstein* Solid State Spectrometer observations of the Orion belt stars. Their data were consistent with the wind shock model of Lucy (1982) but required shock parameters out of the range predicted by the model. This star has also been observed by *ROSAT* (Haberl & White 1993) and *ASCA* (Corcoran et al. 1994). These observations indicated some agreement with the distributed wind shock model. Their fitting procedures indicated the presence of some absorption caused by the stellar wind, but not as much as would be expected if the X-rays originated at the base of the wind.

Most of the modeling effort for early-type stars has been directed toward explaining the four main observables of low resolution (i.e., $E/\Delta E \leq 20$) X-ray spectra: the temperature distribution, the amount of wind absorption, the time variability of the X-ray flux, and the overall flux level. In addition to using this *Chandra* observation to address these issues, this study focuses on new ways to test the distributed shock model for this star. The Medium Energy Grating (MEG) of the High-Energy Transmission Grating Spectrometer (HETGS) has a spectral resolution ranging from $\lambda/\Delta\lambda \approx 300$ for Si XIV at 6.18 Å up to $\approx$1000 for N VII at 24.78 Å (*Chandra* X-Ray Center 2000). Such resolution allows the use of line ratios to measure the radial distribution of the hot gas (a new test of a key prediction of the wind shock models) and the use of emission-line profile shapes to understand the motions of the X-ray–emitting material and the absorption those X-rays undergo.

In the distributed wind shock model, the X-ray–emitting regions are carried out by the rapidly expanding winds of these early type stars. Therefore, the Doppler effect should result in a measurable broadening of the X-ray emission lines. This line broadening has in fact been observed in high-resolution X-ray spectra of a number of hot stars, including

ζ Pup (Cassinelli et al. 2001; Kahn et al. 2001) and ζ Ori (Waldron & Cassinelli 2001). The line profiles of the O star θ^1 Ori C were also observed to be broadened (Schulz et al. 2000), but the apparent importance of large-scale magnetic structures in this extremely young star (Donati et al. 2002) makes it difficult to use as a point of comparison for δ Ori. The broadening observed in all these stars makes them particularly interesting X-ray targets: They comprise one of the few classes of X-ray objects whose line shapes can be resolved and analyzed using the current generation of X-ray instrumentation.

If the X-ray emission were originating in a spherical shell, simple geometric arguments indicate that the emission-line profiles would be flat-topped and symmetric about $v = 0$. If one then considers wind absorption, it is clear that the redshifted X-rays that come from the far side of the wind should suffer more wind attenuation than the blueshifted X-rays that originate nearer the observer. This effect is clearly seen in ζ Pup (Cassinelli et al. 2001; Kahn et al. 2001), whereas the line profiles of ζ Ori are surprisingly symmetric (Waldron & Cassinelli 2001).

A number of recent studies of theoretical X-ray emission-line shapes have been carried out to aid in the interpretation of the newly available X-ray line profiles (Ignace 2001; Ignace & Gayley 2002; Owocki & Cohen 2001). This observation of δ Ori will contribute to these modeling efforts by adding to the quite limited sample of early-type stars whose line profiles have been resolved.

We begin by describing our observation in § 2 and giving an introduction to the δ Ori system while discussing possible sources of X-ray emission for δ Ori in § 3. We then discuss the shapes of individual line profiles in § 4.2, including a discussion of the role of line optical depth (§ 4.3). We constrain the radial location of the X-ray–emitting gas using emission from He-like ions (§ 4.4). Turning to the temperature structure of the gas, we use the measured fluxes of all the strong lines in our observation to estimate the emission measure (EM) of the X-ray–emitting gas (§ 5.1) and then construct ratios of lines of H- and He-like ions as an additional way of measuring the temperature structure of the gas (§ 5.2). We conclude in § 6 with a discussion of what these different measurements imply about the locations and motions of the X-ray–emitting gas in δ Ori's wind.

2. OBSERVATIONS

A 49.0 ks observation of δ Ori A using the *Chandra* HETGS was obtained on 2000 January 13 from $3^h17^m29^s$ to $17^h39^m37^s$ UT. The combined MEG $+/-$ first-order spectrum is shown in Figure 1. The High Energy Grating (HEG) spectrum, which was taken concurrently, is significantly weaker (988 vs. 5870 counts in the MEG) and will not be discussed further here.

We find that many of the dominant lines (H-like, He-like, and several Fe XVII lines) seen in our δ Ori spectrum are similar to those observed in other *Chandra* O star spectra (e.g., Cassinelli et al. 2001; Waldron & Cassinelli 2001). However, the emission lines of δ Ori are noticeably narrower than those of the other stars. The narrowness of these lines allows us to identify many of the weaker lines that were not visible in other O star spectra whose greater line breadth caused the weaker lines to wash out into an indistinguishable "pseudo-continuum." Many iron ions are represented (ranging from Fe XVII to Fe XXI), with peak formation temperatures spanning 5 to 13 million K (MK). Although seen in the spectrum of the O star ζ Pup, the S XV lines near 5.04 Å are not

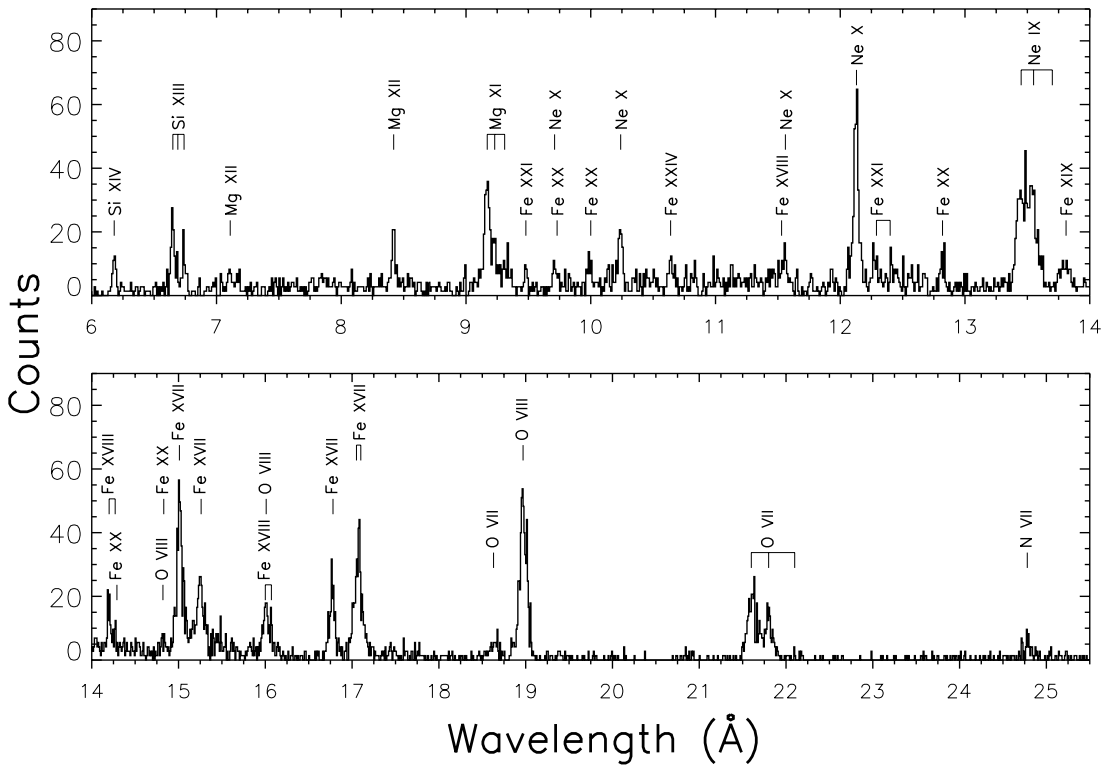

FIG. 1.—Co-added first-order *Chandra* HETGS MEG count spectrum of δ Ori. The ions responsible for the strongest line emission are identified. Note especially the three-line *fir* complexes of O VII, Ne IX, Mg XI, and Si XIII. The bin size is 0.01 Å.

detected in this spectrum. There are in fact very few counts in this spectral region. The S XV line complex was faintly present in the *ASCA* spectrum of δ Ori (Corcoran et al. 1994), and its absence here is probably only due to this observation's relatively short exposure time.

3. THE δ ORI SYSTEM

3.1. *The Three Components*

The δ Ori stellar system consists of three visual components, δ Ori A, δ Ori B, and δ Ori C. Although δ Ori B and C fall within the HETGS field of view (and would be easily resolved by *Chandra*), they show no evidence of any significant X-ray emission and so will no longer concern us here. The source δ Ori A (Mintaka, HD 36486) appears as a single point source on our *Chandra* X-ray image, but it actually consists of three stars. Over the years, this stellar system has been studied intensively both photometrically (Koch & Hrivnak 1981) and spectroscopically (Harvin et al. 2002). Our adopted parameters for the stars' physical characteristics, winds, and orbits are listed in Table 1. In brief, the primary (O9.5 II) and the secondary (B0.5 III) eclipse each other during their 5.7 day orbit (Koch & Hrivnak 1981). According to the ephemeris of Harvin et al. (2002), our observations span roughly 0.39–0.49 in orbital phase. Because primary eclipse was centered on phase 0.95 at the epoch of our observation, that phase range indicates that our observations occurred as the secondary began passing behind the primary. In addition, a distant tertiary star (probably an early B-type star; Harvin et al. 2002) was detected visually by Heintz (1980) and has been confirmed through speckle interferometry (McAlister et al. 1983).

3.2. *X-Rays from Wind Collisions*?

In a multiple star system containing early-type stars, the region in which their strong stellar winds collide is one possible source for the X-ray emission. In the δ Ori system, the tertiary is much too distant from the other two stars to produce any significant X-ray emission from a colliding wind shock. The secondary is much closer to the primary (see Table 1), which requires us to look at the collision between these winds in greater detail.

The location of the wind collision shock can be estimated by determining the point on the line connecting the two stars where the wind momenta balance (Stevens, Blondin, & Pollock 1992). This requires knowledge of the wind properties of the two stars. For the primary, we use direct measurements for the δ Ori system by Lamers & Leitherer (1993), assuming the primary will dominate the measured properties of the system. To determine the wind properties of the secondary, we note that in their Doppler deconvolution of the spectrum of δ Ori A, Harvin et al. (2002) reported that the secondary has a spectrum similar to ϵ Per (B0.5 V). We therefore use this star as a proxy for the secondary star and adopt the stellar wind parameters for ϵ Per from Wilson & Dopita (1985).

Using these values, we find that the wind momenta will balance either at the surface of the secondary or just above it. At that point, the primary's wind is still undergoing significant acceleration and has reached $\approx$60% of its terminal velocity. With these facts in hand, we can use the analytical approach of Usov (1992) to assess the X-ray flux contribution caused by the wind collisions between the primary and the secondary star. Using his equation (82), we find that the unattenuated X-ray luminosity emitted by the colliding wind shock would be an order of magnitude less than the measured X-ray luminosity of 1.1×10^{32} ergs s^{-1} (Cassinelli & Swank 1983).

In addition to this theoretical estimate, there are observational reasons to believe that the colliding wind shock is not the dominant contributor to the system's X-ray output. When δ Ori's L_X/L_{bol} ratio was measured using *ROSAT* by Berghöfer, Schmitt, & Cassinelli (1996), it was typical of other stars in its class (Berghöfer et al. 1997), suggesting that no additional X-ray source is needed to explain its X-ray flux. This view is borne out by the analysis of δ Ori's *ROSAT* X-ray light curve by Haberl & White (1993), which found no variability attributable to orbital modulation. The reanalysis of the *ROSAT* data by Corcoran (1996) indicates

TABLE 1
ADOPTED STELLAR PARAMETERS

Property[a]	Primary	Secondary[b]	Tertiary	Reference
Distance from Earth (pc)	360	...	...	1, 2
Distance from primary ($R_\odot$)	...	33[c]	$\approx 2.5 \times 10^4$[d]	2
Spectral type	O9.5 II	B0.5 III	Early B	2
Orbital period	...	5.7325 days	$\approx$200 yr	2
Radius ($R_\odot$)	11[c]	4[c]	...	2
Mass ($M_\odot$)	10.3[c]	5.2[c]	$\approx$23[e]	2
Optical flux contribution[f] (%)	70	7	23	2
T_{eff} (K)	33,000	27,000	...	3, 4
log g	3.4	3.8	...	3, 4
v_∞ (km s^{-1})	2000	1500	...	5, 6
$\dot{M}$ ($M_\odot$ yr^{-1})	1.07×10^{-6}	1.25×10^{-7}	...	5, 6

[a] Empty entries are not relevant to our analysis.
[b] ϵ Per is used as a proxy for this star, following Harvin et al. 2002.
[c] These values are midway between those derived for the $i = 67°$ and $i = 77°$ cases of Harvin et al. 2002.
[d] From Kepler's law, applied to the tertiary's orbit.
[e] An average of the values in Harvin et al. 2002.
[f] An estimate of the contribution of each component to the system's total optical light output.

REFERENCES.—(1) Brown, de Gevs, & de Zeeuw 1994; (2) Harvin et al. 2002; (3) Voels et al. 1989; (4) Tarasov et al. 1995; (5) Lamers & Leitherer 1993; Wilson & Dopita 1985.

that although δ Ori's X-ray output was somewhat variable, it was not phase-locked in the manner of four of the binaries examined whose *ROSAT* flux was clearly linked with orbital phase. The observations presented here have a more limited phase coverage, but in our analysis of the light curve of the system, we also find no clear evidence of nonrandom variability (see § 3.3). Perhaps a longer *Chandra* observation in the future will be able to demonstrate minor orbital variations in X-ray properties, but the above considerations indicate that it is unlikely that the bulk of the X-rays are coming from a shock in which the winds of the primary and secondary collide.

3.3. *X-Ray Light-Curve Analysis*

Our observation has only a very limited phase coverage ($\approx$0.10 of the binary orbit), so it would be difficult to detect any orbitally modulated variation in δ Ori's X-ray output. Nonetheless, our observations occur at an interesting time when the secondary is passing behind the primary, so it is still worth looking for any change in the X-ray output caused by changes in the colliding wind shock geometry (i.e., the occultation of part of the colliding wind shock by the primary star). Theoretical analysis for orbitally modulated X-ray emission from a binary star system can be found in Pittard & Stevens (1997). As can be seen from the X-ray light curve of our observation (Fig. 2), there is no clear change in the X-ray output of δ Ori during our observation. A maximum likelihood analysis of the light curve in Figure 2 is constant at the 30% confidence level (χ^2 of 1.16). The counts are grouped into 4000 s bins because any shorter bins would result in an unacceptably low signal-to-noise ratio caused by the low X-ray count rate for this star.

The lack of any obvious strong variability during our observation also has implications within the wind shock paradigm. The one-dimensional models of Feldmeier et al. (1997b) indicate that at any given time the majority of the X-ray emission from a star originates in one or two large shocks that grow and fade on a timescale of about 500 s. Such activity should certainly result in some variability on the 4000 s timescale sampled here. *ROSAT* data allowed binning in 400 s intervals for this star (Haberl & White 1993), but no significant variability was seen in that observation either. The conventional explanation for the discrepancy between the highly variable models for these stars' winds and their surprisingly constant X-ray flux involves picturing the one-dimensional Feldmeier et al. (1997b) model as applying to a narrow sector of the wind with very small extent in θ and ϕ (using standard spherical coordinates). The summed contributions of hundreds or thousands of independent sectors would tend to have very little variability even if the individual sectors were highly variable (for a detailed discussion, see Berghöfer & Schmitt 1994). A definitive examination of this result will be possible only when computational capabilities allow full three-dimensional modeling of these winds, although an initial analysis has been performed by Oskinova et al. (2001). The relative constancy of hot star X-ray fluxes has long been known (e.g., Cassinelli & Swank 1983), and in this observation of δ Ori's variability we find nothing to contradict the conclusion that the X-rays arise from many fragmentary wind shocks.

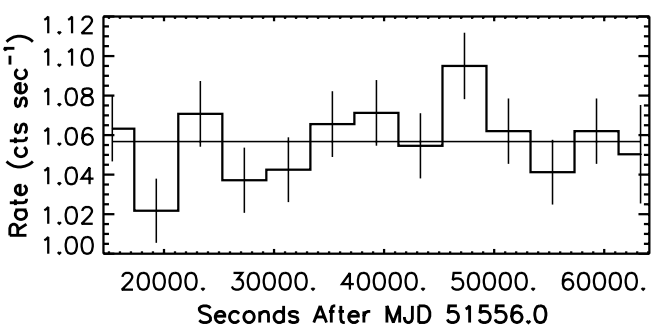

FIG. 2.—X-ray light curve of δ Ori resulting from binning the valid events in all nonzeroth orders (the zeroth-order counts are ignored to avoid problems with photon pileup effects). The errors reflect Poisson statistics on the count numbers in each 4 ks bin. The horizontal line shows the mean count rate of 1.056 counts s^{-1}.

3.4. *What Are the Contributions of the Individual Stars to δ Ori's X-Ray Output*?

In this triple star system, it is important to assess the relative contribution of each star to the system's total X-ray output. The measured optical fluxes of the three stars (Harvin et al. 2002) indicate that the primary star dominates the total visible light output of the system (see Table 1), being responsible for $\approx$70% of the total optical flux from the system. Because the bolometric correction is greater for the primary (a late O star) than for the secondary and tertiary (both early B stars), the primary is responsible for an even greater fraction of the system's bolometric luminosity. Following Haberl & White (1993), the individual stars' X-ray contributions can be estimated using the $L_X \sim 10^{-7} L_{bol}$ relation for early-type stars (Berghöfer et al. 1996). As a caveat, there are indications that there has been Roche lobe overflow in the close binary system (Harvin et al. 2002), so it is not known to what extent those two stars conform to normal star properties. Nonetheless, this analysis indicates that at least 75% of the observed X-ray emission arises from the primary. Furthermore, there is a more rapid drop in X-ray emission starting at early B stars (Cohen, Cassinelli, & MacFarlane 1997), suggesting that the tertiary might contribute even less X-ray flux to the system's total output than the ratios of bolometric magnitudes would indicate. Hence, the remainder of our analysis will assume that the majority of the observed X-ray emission is associated with the primary star.

4. THE LOCATION OF THE X-RAY–EMITTING GAS

4.1. *Line-fitting Procedure*

The high resolution of the *Chandra* and *XMM-Newton* X-ray observatories provides the capability to carry out detailed spectroscopy on a variety of galactic and extragalactic X-ray sources, which, prior to the launch of these satellites, was only functionally possible on solar spectra. Although cool stars are revealing emission-line spectra similar to the Sun, the emission-line spectra of OB stars have generally exhibited very broad lines, and in some cases, these lines show substantial blueshifted line centroids.

In the following sections we discuss several emission-line diagnostics that can be applied to the HETGS data to obtain constraints on the relevant X-ray parameters: line profile characteristics (HWHM and centroid shifts), temperature, EM, and X-ray location in the stellar wind. To extract this information, we calculate the total line energy

flux for each individual line by assuming that the intrinsic line shape is determined by a Gaussian profile superposed on a bremsstrahlung continuum (the line fits are found to be relatively insensitive to our choice of continuum temperature). This approach provides us with an immediate model-free parameterization of the flux, Doppler broadening, and centroid shift of the analyzed emission lines and has the advantage of not requiring any geometric assumptions. The resulting fits can be visually compared with the data to reveal any strong asymmetries in the line shapes.

Waldron & Cassinelli (2001) provided the first attempt to fit a stellar wind distribution of X-ray emission to an HETGS emission line from the O supergiant, ζ Ori. They found that this model could not explain the line profile, and in fact, the best fit to the line was obtained by using a Gaussian line shape. Even for lines that were clearly blueshifted (i.e., those of ζ Pup), it was found that the data could still be described by blueshifted Gaussian line profiles (Cassinelli et al. 2001). Our primary purpose here is to derive the basic observational characteristics of the lines without relying on any specific model a priori. We then discuss these results in the context of the various models for stellar wind X-ray line profiles that have been developed.

The model Gaussian line profiles are folded through the instrumental broadening using the redistribution matrix file (RMF) and area auxillary response file (ARF). We use χ^2 statistics to determine the best-fit line parameters (flux, HWHM, and line centroid) by simultaneously fitting both the MEG $+1$ and -1 spectra. For the case of fitting the blended He-like line complexes (discussed in § 4.4), the fitting procedure includes all three lines simultaneously. All three lines are assumed to have a common HWHM and centroid shift, but the flux of each line is independently determined.

4.2. *Line Profile Analysis*

As mentioned in the introduction, the profile shapes of lines give important clues to the location of the X-ray–emitting regions in an accelerating wind and also the amount of wind absorption the line emission undergoes. In their parameterized study of X-ray emission-line profiles, Owocki & Cohen (2001) define a characteristic wind optical depth of $\tau_* = \kappa \dot{M}/4\pi v_\infty R_*$, which is a measure of the amount of wind absorption expected in a stellar wind. Here κ is the absorption cross section per unit mass, $\dot{M}$ is the stellar mass loss rate, and v_∞ is the wind terminal velocity. We have calculated relative characteristic wind optical depths for O stars that have been observed with *Chandra* using the values in Table 1 for the wind of δ Ori and the measurements in Lamers & Leitherer (1993) for the winds of ζ Ori and ζ Pup. It should be noted that ζ Ori is a binary (Hummel et al. 2000), but the secondary is much dimmer than the primary, so we again assume that the secondary's X-ray contribution can probably be neglected. This characteristic wind optical depth analysis indicates ζ Ori would have a τ_* 8/10 that of δ Ori, while ζ Pup would have a τ_* 1.4 times larger than that of δ Ori. Thus, δ Ori might be expected to have line profile shapes midway between those two cases. This analysis, along with a comparison of the wavelength-dependent wind optical depth (see our § 4.4 and Fig. 2 of Cassinelli et al. 2001) indicate that while δ Ori's wind is thin in photoabsorption for some of the high-energy lines, the wind of ζ Pup is thick in photoabsorption for all observed lines. One may therefore anticipate some differences between these two stars' line profile properties, especially for the high-energy lines.

For the analysis of line profiles in δ Ori, we have selected the strongest relatively isolated lines. In this spectrum, these are the Lyα lines of H-like elements and two lines of Fe XVII. In addition, the relatively weak N VII (24.78 Å) is included in our analysis because it is an important line for estimating conditions far out in the stellar wind (see the discussion in Cassinelli et al. 2001) and for comparisons with previous measurements of other stars. Table 2 lists the measured intrinsic properties of the lines, and Figure 3 compares the fitted results with the observed line profiles.

These lines have line profile shapes consistent with a centroid shift of nearly zero (the weighted average is 0 ± 50 km s^{-1}) and show intrinsic broadening of 430 ± 60 km s^{-1} HWHM, much less than δ Ori's terminal velocity of 2000 km s^{-1}. Such a narrow line width is particularly surprising because the line widths of ζ Ori (a star with a similar terminal velocity of 2100 km s^{-1}) were 1000 ± 240 km s^{-1} HWHM (Waldron & Cassinelli 2001). The line profiles of δ Ori also differ markedly from those of ζ Pup (Cassinelli et al. 2001), in which almost all of the strong lines were both broad (HWHM 850 ± 40 km s^{-1}, $v_\infty = 2200$) and showed a measurable centroid blueshift. Expressing the HWHM of the emission lines as fractions of the stars' terminal velocities yields 0.22 ± 0.03 for δ Ori, 0.48 ± 0.10 for ζ Ori, and 0.38 ± 0.02 for ζ Pup. So, instead of being an intermediate case, δ Ori's emission lines are the narrowest of the three stars discussed.

There is also a slight suggestion of an increase in HWHM for these lines as a function of wavelength (ignoring N VII because of its weak signal). This may be related to the fact that continuum absorption prevents long-wavelength X-rays from escaping from the region near the star (see § 4.4). This would cause more of the X-ray flux for the low-energy lines to originate far from the star where the wind velocity is higher, resulting in broader lines. It is, however, surprising that the lines remain so symmetric if that is the case.

Even with the trend of increasing line width with increasing wavelength, the low energy lines of δ Ori are still much narrower than the corresponding lines observed in ζ Pup. This is somewhat surprising because both stars' winds are optically thick in photoabsorption in this spectral region and so might be expected to produce similar line profiles.

An emission-line profile similar to the flat-topped profile expected from an optically thin shell was clearly seen for the N VII line in ζ Pup (Cassinelli et al. 2001; Kahn et al. 2001),

TABLE 2
LINE PROFILE WIDTHS AND CENTROID SHIFTS

Ion	$\lambda_{\rm rest}$ (Å)	$\mathscr{F}_{\rm line}$[a]	Intrinsic HWHM (km s^{-1})	Centroid Shift (km s^{-1})
Si XIV.....	6.18	0.14 ± 0.11	450 ± 200	-40 ± 600
Mg XII	8.42	0.12 ± 0.07	190 ± 90	-110 ± 300
Ne X	12.13	1.1 ± 0.2	420 ± 170	-150 ± 100
Fe XVII.....	15.01	1.9 ± 0.4	510 ± 220	-50 ± 100
Fe XVII.....	16.78	1.1 ± 0.4	420 ± 250	100 ± 150
O VIII.....	18.97	6.0 ± 0.8	700 ± 100	60 ± 100
N VII.....	24.78	0.7 ± 0.2	420 ± 870	120 ± 400

[a] Line flux in 10^{-13} ergs cm^{-2} s^{-1}.

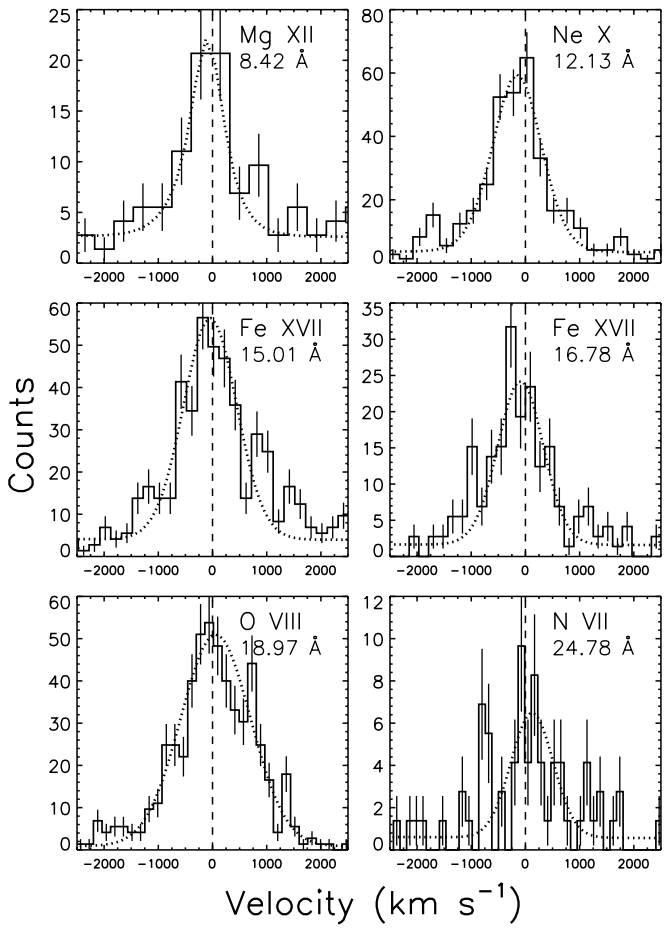

FIG. 3.—MEG co-added first-order X-ray line profiles (*solid*) and Gaussian fits (*dotted*) for six of the brightest lines in the δ Ori spectrum. The vertical dashed lines indicate the rest wavelength for these transitions, and Poisson errors are indicated by error bars. The lines are mostly symmetrical about line center, and all show Doppler broadening. The bin size is 0.01 Å. Parameters for these line fits are given in Table 2.

but none of the lines observed here has a similar shape. In particular, the N VII line from δ Ori does not seem to have a shape appreciably different from any of the other lines, although there are not enough counts to allow a definitive determination.

Comparing the observed HWHM values with δ Ori's wind terminal velocity value of 2000 km s^{-1} might indicate that the major X-ray–emitting zones of this star are near the star where the wind velocity is much less than the terminal velocity. This would be similar to the "base coronal" models, which were among the first explanations for X-rays from hot stars (Cassinelli & Olson 1979). However, the large amount of emission redward of line center observed here would be difficult to explain in this model: with the X-ray emission occurring very close to the star's surface, we would expect to observe a nearly total lack of X-ray emission redward of line center caused by occultation by the star's disk (see Fig. 2 of Ignace 2001). The only way to avoid this effect would be to have downward-flowing material on the near side of the star, although it must be noted that such high negative velocities require acceleration greater than that provided by stellar gravitation (Owocki & Cohen 2001). Thus, these motions would require some other mechanism to accelerate material back toward the star, perhaps something such as magnetic reconnection (Waldron & Cassinelli 2001).

Within the more standard distributed wind shock paradigm, there are a number of models involving different kinds of wind opacity that may (with careful parameter choices) ameliorate some of the discrepancy between the observed line profiles and theoretical expectations. In the line profile modeling by Owocki & Cohen (2001), they find that when varying a wide variety of parameters (wind velocity law β, X-ray onset radius, wind filling factor, radial power law, and wind continuum optical depth), the vast majority of synthesized profiles for distributed wind shock models result in profiles that are blueshifted and strongly asymmetric. They are able to generate relatively broad, unshifted profiles similar to those observed here only if wind attenuation is negligible and the X-ray onset radius is far out in the wind (to prevent asymmetry caused by occultation by the stellar core). Because these broadened, symmetric profiles are what we see for δ Ori, their analysis would indicate either that the wind of δ Ori is strongly clumped (making it relatively "porous" to X-rays) or that the mass-loss rate for δ Ori has been overestimated. They discount the possibility that the low wind photoabsorption could be due to changes in the ionization conditions in the wind because that would strongly interfere with the radiative driving of wind material.

Strong wind clumping for a hot star wind was inferred in an X-ray and UV analysis of τ Sco (B0 V) by Howk et al. (2000). We know that the radiative instability in hot star winds breaks the wind into a series of small-scale shocks. The lack of variability observed in these stars also suggests that the shocks have very limited angular extent. If the wind is sufficiently clumped by these processes, it will become porous to X-ray, and their mean free path will approach the scale of the wind as a whole. Even the X-rays from the far side of the star will escape relatively unattenuated, restoring line profile symmetry. Perhaps future line-profile modeling efforts will consider this effect in a more detailed fashion.

In an alternative explanation, Ignace & Gayley (2002) are able to restore some symmetry to X-ray line profiles by introducing line optical depth effects caused by resonance scattering. In brief, they hypothesize that because of the elongated shape of the Sobolev line interaction region for the wind material that has nearly reached terminal velocity (see Lamers & Cassinelli 1999, Fig. 8.6), the X-rays can escape more easily laterally than radially from the X-ray emission region. This effect would tend to emphasize X-ray emission from regions of the wind with low line-of-sight velocity while suppressing the extremely red- and blueshifted emission. The strongest lines in the spectrum (which have been chosen for analysis here because of their high signal-to-noise ratio) would be the first lines to show this effect. In the limit of strong line optical depth effects, they derive a blueshift in the peak of the line to $v_z = -0.24v_\infty$ and a line HWHM of $0.63v_\infty$. For δ Ori, these values would indicate a centroid shift of 480 km s^{-1} and a line HWHM of 1200 km s^{-1}. A comparison with Table 2 shows that the observed values for δ Ori are much lower than these predictions. As illustrated in Figure 3 of Ignace & Gayley (2002), more moderate line optical depths may slightly lessen the expected centroid shift, but none are able to remove it completely. More importantly, all of their models seem to predict a greater the line broadening than that observed here. It therefore does not seem likely that line optical depth effects

give a straightforward explanation for the line profile shapes seen here. Nonetheless, in § 4.3 we apply an independent method of determining the importance of resonance line scattering in our observation.

A third explanation for the relatively symmetric X-ray line profiles using the properties of individual shocks is also interesting, although it has not yet been subjected to quantitative modeling. In the simulations of wind instability by Feldmeier et al. (1997b), the vast majority of the X-ray emission occurs when small, fast-moving cloudlets run into the starward face of larger, slower moving shocks. The X-rays emitted in the direction away from the star immediately have to pass through all the material of their natal shock, resulting in strong absorption, while those X-rays emitted in a negative radial direction (but not, of course, directly toward the disk of the star) do not have to pass through much of the material of that shock. This effect would act to suppress the blue side of the line profile, tending to counterbalance the effect on line shape caused by the absorption of X-rays from the far side of the star. The geometrical arrangement leading to this effect is most clearly illustrated in Figure 2 of Feldmeier (2001). A determination of the relevance of this mechanism must await global modeling of its overall effect on line profile shapes.

4.3. *Testing for Line Optical Depth Effects*

Determining the importance of strong line optical depth effects caused by resonance scattering is useful both because of its importance in the line profile analysis of Ignace & Gayley (2002) and its possible effects on the observed fluxes of strong lines. For a more detailed discussion, see Brickhouse et al. (2000).

While continuum absorption is due to the cool component, which makes up the majority of the wind, line optical depth caused by the hot, X-ray–emitting component of the wind can be important because resonance transitions have such high oscillator strengths (Ignace & Gayley 2002). It is important to emphasize that resonance scattering simply redirects the photons without destroying them. It can thus be important overall only if a significant number of photons are backscattered into the photosphere (which is only likely to happen near the star), or if repeated line scatterings increase the average X-ray photon path lengths so much as to increase the amount of continuum absorption they suffer. It is therefore important to note that the mechanism described in Ignace & Gayley (2002) could be acting through photon redirection, even if there is not enough photon destruction to be detected here.

A relatively straightforward way to test for line optical depth effects is to compare two lines originating from the same ion that have quite different oscillator strengths. Because both lines originate from the same ion, the emission-line ratio should be unaffected by uncertainties in abundances or ionization fractions. Any line optical depth effects would then be manifested through a diminution of the stronger line with respect to the weaker line in comparison with the known ratio of the lines emitted from an optically thin plasma. One such pair in the *Chandra* passband is the lines of Fe XVII at 15.01 and 15.26 Å (Waljeski et al. 1994). Because it is one of the strongest lines in the spectrum (see Table 2), the Fe XVII line at 15.01 Å would be expected to show line optical depths if any are present. In contrast, the 15.26 Å line is weak enough so that it is unlikely to be affected by line optical depth effects. The 15.01 Å/15.26 Å line ratio is expected to be $\approx$3.5 in an optically thin plasma for a wide range of temperatures based on the APEC/APED plasma emission code (Smith & Brickhouse 2000). The 15.26 Å line has a flux of $(8 \pm 4) \times 10^{-14}$ ergs cm^{-2} s^{-1}, resulting in the line flux ratio $I_{15.01}/I_{15.26} = 2.4 \pm 1.3$. This value would indicate that some line optical depth may be affecting the strongest lines in this observation, although this is not a particularly strong result, because the error range includes the optically thin ratio value of 3.5. We are thus unable to say with certainty that line optical depth plays a strong role in determining line profile shapes, although it certainly appears possible that there is some effect.

4.4. *Emission from Helium-like Ions*

Recent studies of OB stars have employed a powerful new diagnostic for determining the location of the X-ray–emitting gas for these stars by utilizing the forbidden ($3S_1 \rightarrow {}^1S_0$), intercombination ($3P \rightarrow {}^1S_0$), and resonance ($1P_1 \rightarrow {}^1S_0$) (*fir*) transitions of He-like ions (Waldron & Cassinelli 2001; Kahn et al. 2001; Cassinelli et al. 2001). The f/i ratio is modified by exposure to the strong UV fluxes from early-type stars because of the radiative excitation $3S_1 \rightarrow {}^3P$. This weakens the f line and strengthens the i line (Blumenthal, Drake, & Tucker 1972; Porquet et al. 2001). Given a star's UV radiation field (here, the appropriate Kurucz 1993 model atmosphere is used for the photospheric flux), the expected f/i ratio can be computed for a range of distances from the stellar surface and compared with the observed ratios to determine at what radii the X-rays originate.

As indicated in our δ Ori spectrum (see Fig. 1), four He-like *fir* line complexes are clearly evident (Si XIII, Mg XI, Ne IX, and O VII). However, only Si XIII and Mg XI show measurable f line fluxes. The Ne IX and O VII f lines are strongly suppressed by the radiative excitation process, indicating that we can only establish upper limits on the radii of emission for these ions.

To put these measurements on a more quantitative basis, we fitted each line complex using the technique discussed in § 4.1. The results of this fitting procedure are shown in Table 3, which lists the measured fluxes from each of the three lines in every *fir* complex, the total combined flux, and the resulting f/i ratios.

Following the procedure given by Waldron & Cassinelli (2001), our derived f/i ratios can be used to determine the radial formation regions of the He-like *fir* lines, as illustrated in the top part of Figure 4. We note that in addition to the Poisson errors in the ratio measurement, there is an uncertainty associated with the assumed model UV flux (see, e.g., Chavez, Stalio, & Holberg 1995). This is especially important for the unobservable photospheric flux shortward of 912 Å, which effects the emission from Si XIII. For example, assuming a lower UV flux than that used here will shift all model f/i curves to the left (*lower radii*) in Figure 4, and vice versa for a higher UV flux. Nonetheless, even in the presence of these uncertainties, we can still derive important radial constraints on the X-ray–emitting gas from this analysis.

As discussed in Cassinelli et al. (2001), the X-rays may be expected to originate from near the monochromatic X-ray photosphere, roughly defined as the radius having an opti-

TABLE 3
FLUXES FOR LINES FROM He-LIKE IONS AND f/i RATIOS

Ion	r Flux[a]	i Flux[a]	f Flux[a]	Combined Flux[a]	f/i Ratio
Si XIII.....	0.19 ± 0.05	0.05 ± 0.03	0.11 ± 0.04	0.33 ± 0.14	2.2 ± 1.3
Mg XI	0.28 ± 0.08	0.10 ± 0.06	0.05 ± 0.03	0.43 ± 0.12	0.5 ± 0.4
Ne IX	1.4 ± 0.4	1.5 ± 0.4	0.03 ± 0.2	2.9 ± 0.7	<0.1
O VII.....	4.6 ± 1.1	3.4 ± 1.1	0.2 ± 0.8	8.2 ± 2.0	<0.2

[a] Line flux in 10^{-13} ergs cm^{-2} s^{-1}.

cal depth of unity for each individual X-ray wavelength. This occurs because any X-rays emitted nearer the star than the optical depth of unity surface are unlikely to escape without being absorbed. Conversely, if hot gas is formed throughout the wind, the largest amount of X-ray emission will occur as near the star as possible because density rapidly falls off with radius, and X-ray emission is proportional to the square of the density. The bottom of Figure 4 compares the radii derived from the *fir* procedure to the optical depth of unity for continuum opacity in the wind, using wind opacity modeling of MacFarlane et al. (1993).

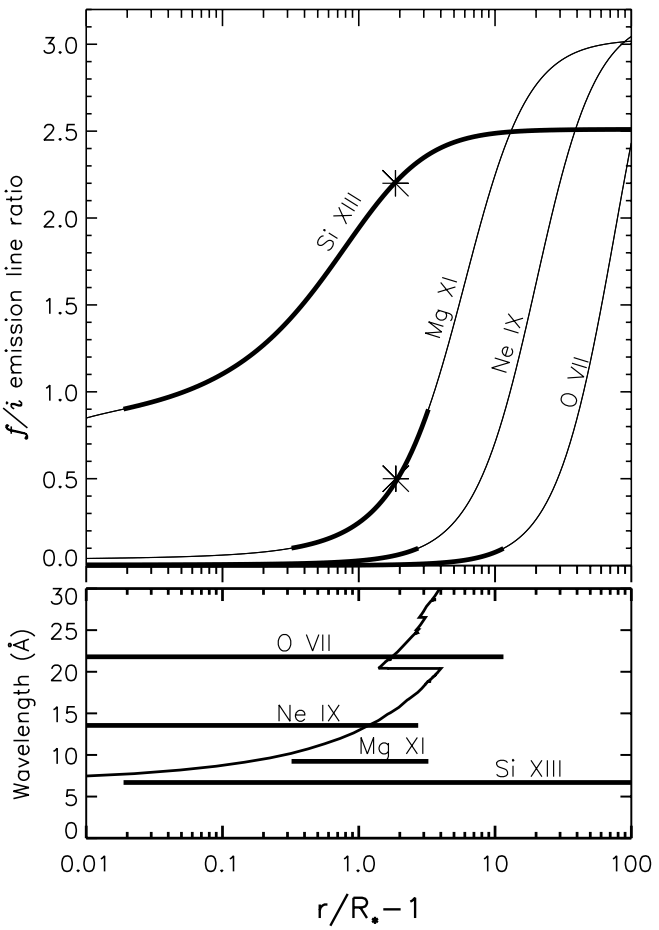

FIG. 4.—Dependence of the O VII, Ne IX, Mg XI, and Si XIII f/i line ratios on radius caused by the geometric dilution of the UV radiation field. The asterisks indicate the measured values, while the darkened lines extend over the range of the uncertainty in the f/i line ratio for each ion. The Ne IX and O VII ions give only upper limits, while the uncertainty for the Si XIII ion extends to arbitrarily high radii. The bottom panel gives the radius of wind continuum optical depth of unity as a function of wavelength. The dark horizontal lines correspond to the ranges in radii indicated by the f/i ratios of the top panel.

This analysis indicates it is likely that the observed O VII and Ne IX emission originates near the high-radius end of the ranges indicated in Figure 4 because most emission from deep within the wind would be absorbed at those wavelengths. We note in passing the consistency of the O VII and Ne IX measurements with the general wind shock X-ray emission paradigm wherein most of the X-ray emission does not occur at great distances from the star. In the paradigm developed in Feldmeier et al. (1997b), these upper limits on radii indicate that while some hot gas may persist to great distances, cloudlet-shock collisions have ceased.

The emission from Mg XI and Si XIII is more interesting. At these wavelengths, absorption by the stellar wind is weak enough so that we can see nearly to δ Ori's surface. The fact that the f lines are not fully suppressed from these ions indicates that there is not much X-ray emission near the wind base, although the weakness of these lines makes a precise measurement difficult.

If the X-ray emission originates at these radii (where the wind has reached an appreciable fraction of v_∞), it is difficult to understand how the X-ray profiles can be so narrow (see § 4.2). A straightforward interpretation would involve shocks containing hot gas at an appreciable distance from the star but with a much slower motion than the ambient cool medium. Such shocks are not present in current simulations of wind instabilities, and it is not clear at present how they could be produced, although a somewhat similar situation involving the cool wind streaming past small pockets of X-ray–emitting gas is discussed for τ Sco in Howk et al. (2000).

It is also interesting to compare the results found here with the study by Cassinelli et al. (2001), who found X-ray emission very near the surface of ζ Pup. That finding was difficult to explain within the standard wind shock paradigm: At those small radii, the wind does not yet have a velocity high enough to create the strong shocks needed to create the required temperatures. We have no such difficulty here. The *fir* analysis for δ Ori indicates the X-ray emission is occurring far enough from the star to allow the wind to have reached velocities that permit shock jumps of the requisite size. The fact that the dominant Mg XI and Si XIII emission regions occur at some distance from the star's surface therefore generally supports the standard wind shock X-ray emission model.

5. THE TEMPERATURE STRUCTURE OF THE X-RAY–EMITTING GAS

5.1. *The Line Emission Measure Distribution*

From the broad sample of lines that show prominent X-ray emission in δ Ori, we can obtain limits on the volume EM as a function of temperature. These EM estimates are

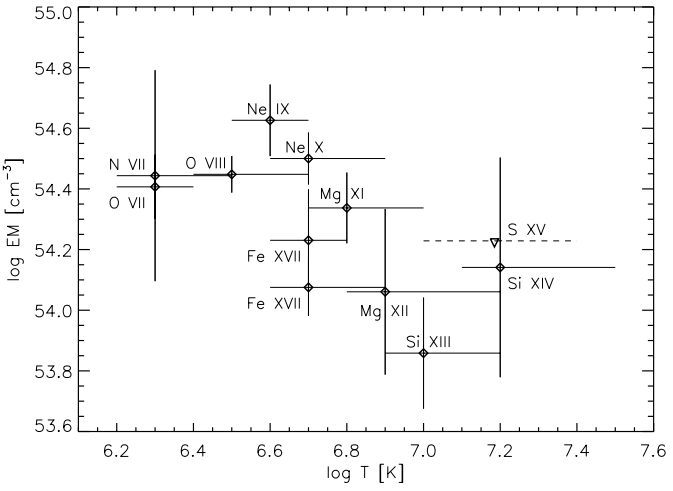

FIG. 5.—Estimated EMs for the strong lines in δ Ori's spectrum vs. the temperature of the line's peak emission. The band in temperature shown for each line corresponds to the range over which it has at least half its peak emission. The detection limit for S XV is indicated by an inverted triangle.

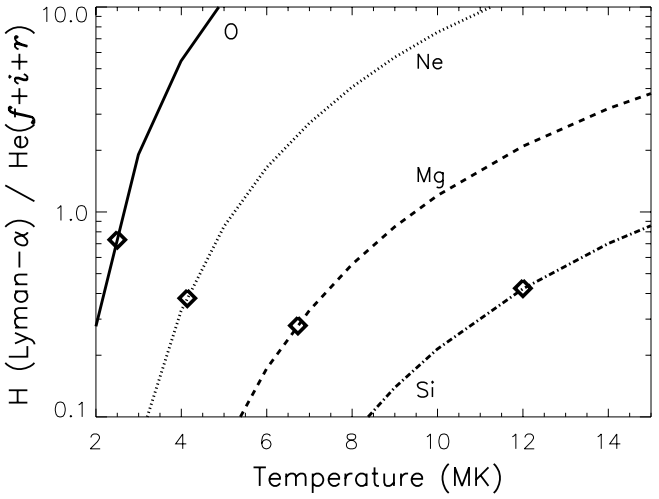

FIG. 6.—Estimating the temperature using ratios of the principal K-shell lines from H- and He-like ions. The thick curved lines are the predicted emission-line ratios as a function of temperature. The diamonds indicate the measured ratios and inferred temperatures for this observation of δ Ori.

derived from the ratios of the measured fluxes of the most prominent lines to their peak emissivities taken from the APEC/APED code (Smith & Brickhouse 2000). The points in Figure 5 define an approximate upper envelope to the true volume EM distribution. This method results in an upper envelope for the distribution because if the true EM were larger than these values, the emission lines would be stronger than what was observed. We have made the necessary minor correction for ISM absorption. This method is discussed in more detail in Kahn et al. (2001), and a comparison of this estimate with more detailed methods for determining the temperature structure of Capella can be found in Figure 3 of Canizares et al. (2000).

The EM versus temperature envelope allows for a broad peak of the X-ray emission near 4 MK with EM_{max} near 4×10^{54} cm^{-3}. For comparison, the EM of the entire wind is roughly 1.8×10^{58} cm^{-3} (determined using the prescription in Cassinelli et al. 1981 and the values in Table 1). This indicates that the X-ray–emitting gas is only a minor constituent of the wind as a whole. The EM envelope can extend to high temperatures, consistent with the large range of ionization states of iron seen. Emission lines with similar temperatures of formation are seen to require similar EMs for all the elements, indicating normal abundances. Even the widest spread (near 5 MK) is well within the uncertainties in predicted line emissivities. This finding of roughly normal abundances is in contrast to the study of ζ Pup by Kahn et al. (2001), in which their Figure 3 indicated a large nitrogen overabundance. If the carbon and oxygen measurements in their Figure 3 are therefore taken to be representative, ζ Pup has an EM distribution that rises with temperature, in contrast with the broadly peaked distribution seen here.

5.2. *Estimating the Temperature Using Lines from* H- *and* He-*like Ions*

In this section we complement the EM analysis of § 5.1 by comparing the brightest K-shell lines of the H- and He-like species of individual elements as an additional measure of temperature structure. As the temperature increases, the ionization balance shifts from He- to H-like ions. This change is reflected in the ratio of the strong lines from these ions. This comparison provides a simple plasma thermometer that has the advantage of being abundance-independent because we are comparing emission lines from ions of the same element. Each pair of ion states is sensitive to a different range of gas temperatures because, for example, Si XIII and Si IV exist only in plasma with much higher temperatures than gas that shows O VII and O VIII emission. For an application of this line-ratio diagnostic to a cataclysmic variable, see Ramsay et al. (2001).

We use the atomic calculations of MacFarlane, Cohen, & Wang (1994) to determine the ratio of the H-like Lyα line of a specific element to the combined fluxes of the *fir* lines from the corresponding He-like ion. Figure 6 shows the line ratios versus temperature. Similar to the findings in § 5.1, this method also indicates a broad range of temperature, ranging from $\approx$2.5 MK for O up to $\approx$12 MK for Si, evidence that there is indeed a wide range of plasma temperatures involved in the observed X-ray emission.

Direct comparisons with previous temperature determinations of the X-ray–emitting gas for this star are somewhat ambiguous because there is a strong dependence on the properties of the detectors used. For example, with the relatively soft PSPC detector on *ROSAT*, Haberl & White (1993) found that a two-temperature fit with components at 1.2 and 2.4 MK was required, while with the SIS detector on *ASCA* had a harder spectral response and required temperature components at 2.9 and 6.9 MK (Corcoran et al. 1994). The overall detector response is less important in the measurements presented here because the entire spectrum is not fitted at once. Rather, the temperature sensitivity ranges for this method occur where the ionization fractions of specific ions are high.

The wide range in temperature found here is generally in accord with what would be expected from a wind shock X-ray source. In this paradigm, individual shocks are constantly growing and fading. An overall measurement of the temperature structure of the hot gas must aggregate the individual contributions of shocks of varying strengths and stages in their development (Feldmeier et al. 1997b). This would lead to a broad temperature distribution similar to that seen here.

6. DISCUSSION AND SUMMARY

The most difficult issue to resolve in this study involves finding an appropriate explanation of the shapes of the X-ray emission lines. The emission lines of δ Ori are only broadened to roughly a quarter of v_∞, which might indicate that the X-ray emission occurs in the regions with low wind velocity. But, if the X-rays originate that close to the star, then why is the redshifted emission not occulted by the stellar disk? In any case, δ Ori's wind should be optically thick in the continuum for many of the X-ray lines. Where is the line asymmetry that would be expected from the absorption of redshifted X-rays originating from the far side of the star?

In order to understand these discrepancies, we have compared our results to a number of the increasingly sophisticated models of X-ray line shapes for these stars. Unfortunately, none of the current models for hot star X-ray line profiles is fully satisfactory in explaining these profiles. Perhaps a more detailed analysis of the effects of clumping in these winds will help future modeling efforts produce profiles that more closely resemble those observed in this star.

Our results for δ Ori's EM, temperature distribution, and flux constancy are in accord with previous measurements for this star. Not surprisingly, these measurements in general support the wind shock model that has been developed to explain previous observations. *Chandra*'s ability to resolve the line complexes of He-like ions adds another measurement into the mix: the emission from He-like ions appears to be coming from moderate radii for this star. This shows general agreement with the expectations of a distributed wind shock model, although it is not clear at this time how this measurement relates to the relatively narrow emission-line profiles observed for δ Ori.

As this study indicates, the high spectral resolutions now available are powerful tools for understanding the X-ray emission from O and B stars. The presence of phenomena not easily explained, such as the X-ray line profiles presented here, should help ensure that hot star X-ray astronomy remains a lively field of inquiry.

We would like to acknowledge support from SAO grants GO0-1090A for N. A. M. and J. P. C., GO0-1075X for W. L. W., GO0-1090B for J. J. M. and D. H. C., and a Wisconsin Space Grant Consortium Fellowship for N. A. M. We would also like to thank the referee for many helpful comments and suggestions.

REFERENCES

Berghöfer, T. W., & Schmitt, J. H. M. M. 1994, A&A, 290, 435
Berghöfer, T. W., Schmitt, J. H. M. M., & Cassinelli, J. P. 1996, A&AS, 118, 481
Berghöfer, T. W., Schmitt, J. H. M. M., Danner, R., & Cassinelli, J. P. 1997, A&A, 322, 167
Blumenthal, G. R., Drake, G. W. F., & Tucker, W. H. 1972, ApJ, 172, 205
Brickhouse, N. S., Dupree, A. K., Edgar, R. J., Liedahl, D. A., Drake, S. A., White, N. E., & Singh, K. P. 2000, ApJ, 530, 387
Brown, A. G. A., de Geus, E. J., & de Zeeuw, P. T. 1994, A&A, 289, 101
Canizares, C. R., et al. 2000, ApJ, 539, L41
Cassinelli, J. P., Miller, N. A., Waldron, W. L., MacFarlane, J. J., & Cohen, D. H. 2001, ApJ, 554, L55
Cassinelli, J. P., & Olson, G. L. 1979, ApJ, 229, 304
Cassinelli, J. P., & Swank, J. H. 1983, ApJ, 271, 681
Cassinelli, J. P., Waldron, W. L., Sanders, W. T., Harnden, F. R., Rosner, R., & Vaiana, G. S. 1981, ApJ, 250, 677
Chandra X-Ray Center 2000, *Chandra* Proposers' Observatory Guide, Version 3.0, TD 403.00.003 (Cambridge: CXC)
Chavez, M., Stalio, R., & Holberg, J. B. 1995, ApJ, 449, 280
Cohen, D. H., Cassinelli, J. P., & MacFarlane, J. J. 1997, ApJ, 487, 867
Cooper, R. G., & Owocki, S. P. 1994, Ap&SS, 221, 427
Corcoran, M. F. 1996, Rev. Mexicana Astron. Astrofis. Ser. Conf., 5, 54
Corcoran, M. F., et al. 1994, ApJ, 436, L95
Donati, J.-F., Babel, J., Harries, T. J., Howarth, I. D., Petit, P., & Semel, M. 2002, MNRAS, 333, 55
Feldmeier, A. 1995, A&A, 299, 523
———. 2001, Ph.D. thesis, Potsdam Univ.
Feldmeier, A., Kudritzki, R.-P., Palsa, R., Pauldrach, A. W. A., & Puls, J. 1997a, A&A, 320, 899
Feldmeier, A., Puls, J., & Pauldrach, A. W. A. 1997b, A&A, 322, 878
Haberl, F., & White, N. E. 1993, A&A, 280, 519
Harvin, J. A., Gies, D. R., Bagnuolo, W. G., Penny, L. R., & Thaller, M. L. 2002, ApJ, 565, 1216
Heintz, W. D. 1980, ApJS, 44, 111
Howk, J. C., Cassinelli, J. P., Bjorkman, J. E., & Lamers, H. J. G. L. M. 2000, ApJ, 534, 348
Hummel, C. A., White, N. M., Elias, N. M., Hajian, A. R., & Nordgren, T. E. 2000, ApJ, 540, L91
Ignace, R. 2001, ApJ, 549, L119
Ignace, R., & Gayley, K. G. 2002, ApJ, 568, 954
Kahn, S. M., Leutenegger, M. A., Cottam, J., Rauw, G., Vreux, J. -M., den Boggende, A. J. F., Mewe, R., & Güdel, M. 2001, A&A, 365, L312
Koch, R. H., & Hrivnak, B. J. 1981, ApJ, 248, 249
Kurucz, R. L. 1993, in IAU Colloq. 138, Peculiar versus Normal Phenomena in A-Type and Related Stars, ed. M. M. Dworetsky, F. Castelli, & R. Faraggiana (San Francisco: ASP), 87
Lamers, H. J. G. L. M., & Cassinelli, J. P. 1999, Introduction to Stellar Winds (Cambridge: Cambridge Univ. Press)
Lamers, H. J. G. L. M., & Leitherer, C. 1993, ApJ, 412, 771
Lucy, L. B. 1982, ApJ, 255, 286
Lucy, L. B., & White, R. L. 1980, ApJ, 241, 300
MacFarlane, J. J., Cohen, D. H., & Wang, P. 1994, ApJ, 437, 351
MacFarlane, J. J., Waldron, W. L., Corcoran, M. F., Wolff, M. J., Wang, P., & Cassinelli, J. P. 1993, ApJ, 419, 813
McAlister, H. A., Hartkopf, W. I., Hendry, E. M., Campbell, B. G., & Fekel, F. C. 1983, ApJS, 51, 309
Oskinova, L. M., Ignace, R., Brown, J. C., & Cassinelli, J. P. 2001, A&A, 373, 1009
Owocki, S. P., Castor, J. I., & Rybicki, G. B. 1988, ApJ, 335, 914
Owocki, S. P., & Cohen, D. H. 2001, ApJ, 559, 1108
Owocki, S. P., & Puls, J. 1996, ApJ, 462, 894
———. 1999, ApJ, 510, 355
Pittard, J. M., & Stevens, I. R. 1997, MNRAS, 292, 298
Porquet, D., Mewe, R., Dubau, J., Raassen, A. J. J., & Kaastra, J. S. 2001, A&A, 376, 1113
Ramsay, G., et al. 2001, A&A, 365, L294
Runacres, M. C., & Owocki, S. P. 2002, A&A, 381, 1015
Schulz, N. S., Canizares, C. R., Huenemoerder, D., & Lee, J. C. 2000, ApJ, 545, L135
Smith, R. K., & Brickhouse, N. S. 2000, Rev. Mexicana Astron. Astrofis. Ser. Conf., 9, 134
Stevens, I. R., Blondin, J. M., & Pollock, A. M. T. 1992, ApJ, 386, 265
Tarasov, A. E., et al. 1995, A&AS, 110, 59
Usov, V. V. 1992, ApJ, 389, 635
Voels, S. A., Bohannan, B., Abbott, D. C., & Hummer, D. G. 1989, ApJ, 340, 1073
Waldron, W. L., & Cassinelli, J. P. 2001, ApJ, 548, L45
Waljeski, K., Moses, D., Dere, K. P., Saba, J. L. R., Strong, K. T., Webb, D. F., & Zarro, D. M. 1994, ApJ, 429, 909
Wilson, I. R. G., & Dopita, M. A. 1985, A&A, 149, 295